

Spatially inhomogeneous competition between superconductivity and the charge density wave in $\text{YBa}_2\text{Cu}_3\text{O}_{6.67}$

J. Choi¹, O. Ivashko^{1,2}, E. Blackburn^{3,4}, R. Liang^{5,6}, D.A. Bonn^{5,6}, W.N. Hardy^{5,6}, A.T. Holmes ⁷, N.B. Christensen⁸, M. Hücker⁹, S. Gerber ¹⁰, O. Gutowski², U. Rütt ², M.v. Zimmermann ², E.M. Forgan³, S.M. Hayden¹¹  & J. Chang ¹ 

The charge density wave in the high-temperature superconductor $\text{YBa}_2\text{Cu}_3\text{O}_{7-x}$ (YBCO) has two different ordering tendencies differentiated by their *c*-axis correlations. These correspond to ferro- (F-CDW) and antiferro- (AF-CDW) couplings between CDWs in neighbouring CuO_2 bilayers. This discovery has prompted several fundamental questions: how does superconductivity adjust to two competing orders and are either of these orders responsible for the electronic reconstruction? Here we use x-ray diffraction to study $\text{YBa}_2\text{Cu}_3\text{O}_{6.67}$ as a function of magnetic field and temperature. We show that regions with F-CDW correlations suppress superconductivity more strongly than those with AF-CDW correlations. This implies that an inhomogeneous superconducting state exists, in which some regions show a fragile form of superconductivity. By comparison of F-CDW and AF-CDW correlation lengths, it is concluded that F-CDW ordering is sufficiently long-range to modify the electronic structure. Our study thus suggests that F-CDW correlations impact both the superconducting and normal state properties of YBCO.

¹Physik-Institut, Universität Zürich, Winterthurerstrasse 190, CH-8057 Zürich, Switzerland. ²Deutsches Elektronen-Synchrotron DESY, 22607 Hamburg, Germany. ³School of Physics and Astronomy, University of Birmingham, Birmingham B15 2TT, UK. ⁴Division of Synchrotron Radiation Research, Department of Physics, Lund University, Sölvegatan 14, 22100 Lund, Sweden. ⁵Department of Physics & Astronomy, University of British Columbia, Vancouver, Canada. ⁶Canadian Institute for Advanced Research, Toronto, Canada. ⁷European Spallation Source ERIC, Box 176, SE-221 00 Lund, Sweden. ⁸Department of Physics, Technical University of Denmark, DK-2800 Kongens Lyngby, Denmark. ⁹Department of Condensed Matter Physics, Weizmann Institute of Science, 7610001 Rehovot, Israel. ¹⁰Laboratory for Micro and Nanotechnology, Paul Scherrer Institut, Forschungsstrasse 111, CH-5232 Villigen, PSI, Switzerland. ¹¹H. H. Wills Physics Laboratory, University of Bristol, Bristol BS8 1TL, UK. ✉email: S.Hayden@bristol.ac.uk; joan.chang@physik.uzh.ch

Many theories and experiments point to an inhomogeneous nature of the superconductivity of high-temperature cuprate superconductors (HTC). Indeed, inhomogeneity in the sense of phase separation, intertwining of competing order parameters, stripes or pair-density-waves^{1–5} may be at the heart of cuprate superconductivity. Underdoped high-temperature superconductors exhibit competing tendencies towards charge-density-wave (CDW) and superconducting (SC) orders^{6–10}. This means that the effects of quenched disorder may induce defects that disrupt or suppress the CDW order, and in turn lead to a resurgence of superconductivity. The application of a magnetic field provides another interesting control parameter because the introduction of vortices into the superconducting state tips the energy balance in favour of CDW order.

In this context, $\text{YBa}_2\text{Cu}_3\text{O}_{6+x}$ (YBCO) is an important model system where large onset temperatures of both superconductivity and CDW order are present^{8,9,11,12}. As a function of both magnetic field and uniaxial stress, two intimately related CDW ordering tendencies have been realised^{13–16}. These correspond to different ordering patterns along the c -axis^{13,14}, as schematically illustrated in Fig. 1. Magnetic field (or uniaxial stress) induces an in-phase ferro-coupled CDW (F-CDW) along the c -axis^{14,15} on top of the original out-of-phase bi-axial antiferro-coupled CDW (AF-CDW) order. Quenched disorder, that in YBCO is naturally introduced through imperfections in the chain layer, may have important implications for the CDW order^{15,17,18}. It is believed that disorder locally favours the AF-CDW order and that the evolution of the CDW correlations with magnetic field may be understood as a crossover transition in which the CDW coupling along the c -axis varies^{14,18}. The introduction of normal vortices with field leads to a more ordered CDW. This suggests disorder associated with vortices is of secondary importance.

More recently, the case where competing tendencies towards CDW and SC order in the presence of topological defects due to quenched disorder and of vortices in the SC state has been considered¹⁷. It was demonstrated theoretically that a fragile SC state can occur at low temperatures and at high magnetic field. This state is based on regions in which the CDW order is weakened due to defects where locally superconducting halos can form. These regions can then couple to form a state with global SC phase coherence. Given the richness of theoretical possibilities when superconductivity competes with CDW order in the presence of vortices and weak disorder, it is of great interest to scrutinise the magnetic field-induced phase competition in YBCO.

Here we present a comprehensive study of the F-CDW and AF-CDW correlations in $\text{YBa}_2\text{Cu}_3\text{O}_{6.67}$. By varying the magnetic field strength B – applied along the crystallographic c -axis – and temperature T , new insights into in-plane correlation lengths in the phase space (B, T) and competition of the correlations with superconductivity are obtained. F-CDW correlations are traced from low fields. From the diffraction intensities of F- and AF-CDW correlations versus temperature and magnetic field, the competition with superconductivity is studied. In particular, we extract the characteristic temperatures below which the respective CDW correlations are suppressed. They are significantly different at high magnetic fields, where the F-CDW correlation length becomes large, and the F-CDW correlations are suppressed at a significantly lower temperature scale. These different temperatures indicate where superconducting order becomes strong enough to influence the F-CDW and AF-CDW correlations. This observation suggests that superconductivity in the F-CDW regions is more strongly suppressed by the CDW. In this fashion, inhomogeneous superconductivity emerges due to competition with CDW correlations which are locally different. Consequently, regions with weaker or more fragile superconductivity are created. Another implication of our study is that in-plane correlation lengths can be deduced across the (B, T) phase space. We extract the in-plane correlation lengths at the field-dependent temperature scales set by the phase competition between superconductivity and the two CDW ordering tendencies. It is demonstrated that the F-CDW in-plane correlation length exceeds that of the AF-CDW order down to magnetic fields as small as 5 T. This result raises the question as to whether F-CDW correlations may be related to the Fermi surface reconstruction. Together with the recent finding that uniaxial strain induces F-CDW order¹⁶, our results suggest that F-CDW order in YBCO plays an important role for both the electronic structure and in rendering superconductivity into an inhomogeneous state that includes a more fragile flavour.

Results

Charge-density-waves in YBCO. Charge density wave (CDW) ordering has been found to be a universal property of hole doped cuprates^{6–9,19–21}. YBCO has a bilayer structure with relatively close ($d = 3.3 \text{ \AA}$) pairs of CuO_2 planes, separated by layers containing CuO chains running along the b -axis. In YBCO, the CDW results in weak scattering centred at $\mathbf{Q}_{\text{CDW}}(\ell) = \boldsymbol{\tau} + \mathbf{q}_{\text{CDW}} + \ell\mathbf{c}^*$, where $\boldsymbol{\tau}$ is a reciprocal lattice point of the unmodulated structure and $\mathbf{q}_{\text{CDW}} = (\delta_a, 0, 0)$ or $(0, \delta_b, 0)$ ^{8,9,11}. For the $\text{YBa}_2\text{Cu}_3\text{O}_{6.67}$

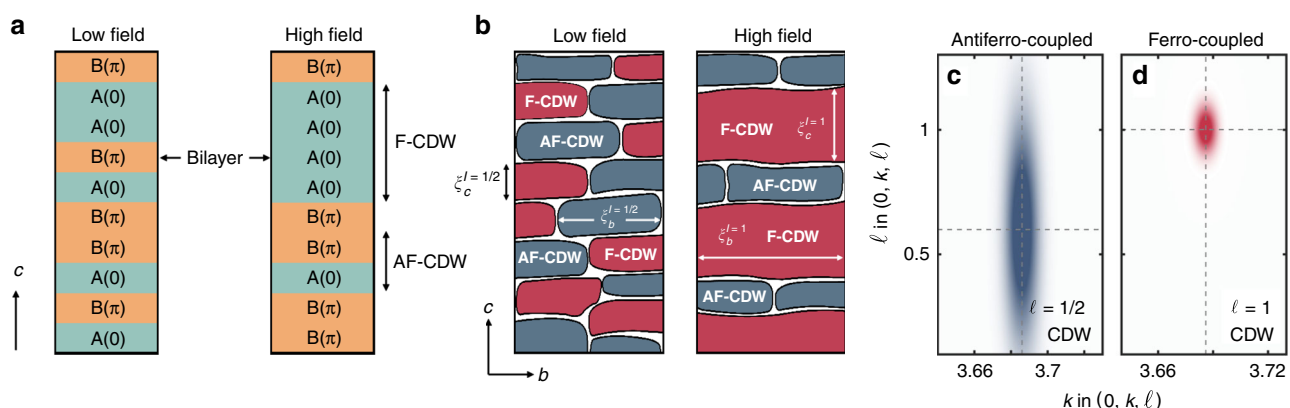


Fig. 1 Schematic real-space illustration of the disordered charge density wave (CDW) in $\text{YBa}_2\text{Cu}_3\text{O}_{6.67}$. **a** Representative CDW stacking sequences along the c -axis at low and high magnetic field for a fixed point in the a - b plane. A and B represent the two possible phases in the CDW modulation in each bilayer¹⁴. **b** Extension to the b - c plane. Spatially separated regions where the F-CDW ($\ell = 1$) and AF-CDW ($\ell = 1/2$) correlations in **a** are present. **c, d** Idealised diffraction intensity for the F-CDW and AF-CDW correlations at high field.

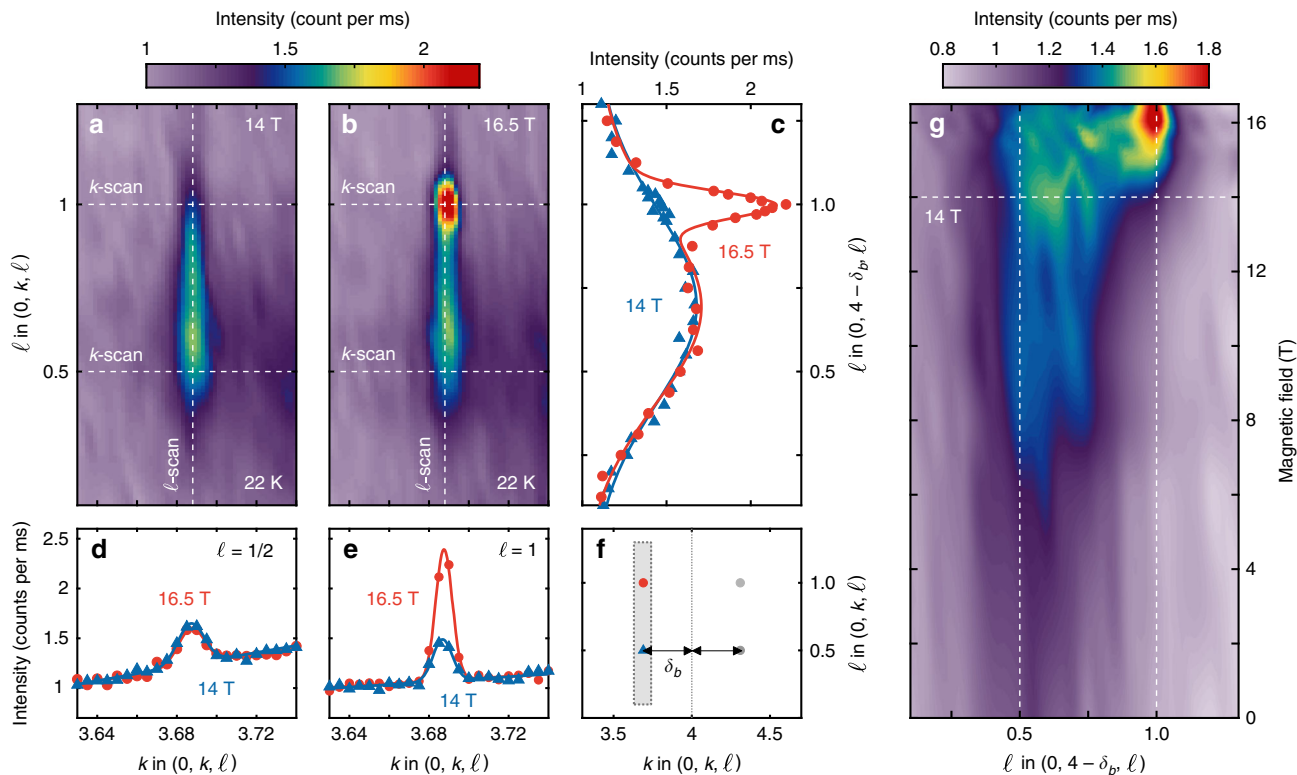


Fig. 2 Magnetic-field-induced correlations and three-dimensional CDW order in $\text{YBa}_2\text{Cu}_3\text{O}_{6.67}$. **a, b** X-ray diffraction intensity maps around $(0, 4 - \delta_b, \ell)$ with $B = 14$ T and 16.5 T, respectively. **c, d, and e** are ℓ - and k -dependent intensity profiles along the vertical and horizontal white dashed lines in **a, b**. **f** Delineation of the scattering plane and probed reciprocal space (grey). The in-plane incommensurability δ_b is defined by the horizontal arrow. **g** Diffraction intensity map displayed in false colour, as a function of ℓ and magnetic field. Source data are provided as a Source Data file.

($T_c = 67$ K) composition studied here, two charge-density-wave components have been identified^{13–15}. The first, found in zero magnetic field, develops below $T_{\text{CDW}} = 140(10)$ K with $\delta_a = 0.305(2)$ and $\delta_b = 0.314(2)$. The phase of this CDW in neighbouring bilayers has an anti-parallel correlation with only weak correlation along the c -axis, manifested by a broad intensity peak with an $\ell \approx 1/2$ modulation. The intensity of these rods of scattering is enhanced by the application of a magnetic field along the c -axis^{9,22,23}. Figure 2a displays this rod in the $(0, k, \ell)$ scattering plane for $B = 14$ T. A second magnetic-field-induced CDW exists along the b -axis direction^{13–15}. This CDW has the same phase across neighbouring bilayers (ferro-coupled) and hence is manifested by a $\ell = 1$ reflection on top of the $\ell \sim 1/2$ scattering rod (see Fig. 1c, d and Fig. 2a, b). In this paper we use the term “CDW order” loosely to mean static CDW correlations with a finite correlation length which develop at low temperatures and high magnetic fields.

Modelling¹⁴ of the c -axis correlations in YBCO suggests that magnetic field changes the inter-bilayer (IB) coupling of the CDW. This is an indirect effect in that the field suppresses the superconductivity which changes the IB coupling. The CDW will also be pinned by defects in the chain layer. Thus, we can view the evolution of the CDW with field as a crossover transition. At low field $B \lesssim 14$ T, the CDW is pinned and the system displays weakly correlated $\ell = 1/2$ order. At very high field ($B \gg 14$ T), in-phase coupling of the bilayers is favoured, which is sufficient to overcome the pinning and forms a state with long range $\ell = 1$ order along the b -axis only.

Two-component analysis. The two CDW orderings can be analysed separately as a function of temperature and magnetic field. Here we employ three separately independent but consistent

methodologies for data analysis. First, as shown in Figs. 2d, e and 3d, e, the in-plane correlations and diffraction intensities can be inferred from Gaussian fits versus Q_b at $\ell = 1/2$ and $\ell = 1$. The correlation lengths are defined as $\xi_b^{\ell=1/2,1} = 1/\sigma_b^{\ell=1/2,1}$ where $\sigma_b^{\ell=1/2}$ and $\sigma_b^{\ell=1}$ are the respective standard deviations. Second, along the $(0, 4 - \delta_b, \ell)$ direction, the out-of-plane correlation lengths $\xi_c^{\ell=1/2,1}$ can be deduced by fitting with a double Gaussian function (Fig. 3c). The centre in ℓ of the broad AF-CDW signal rises slightly with magnetic field¹⁴ (the values that were fitted and at high field were all ~ 0.6), however, for simplicity we label the correlation lengths as $\xi_c^{\ell=1/2,1}$. We find that the temperature dependence of the broad peak is insensitive to the exact ℓ value (see supplementary Fig. 1), and all h - and k -scans were carried out at $\ell = 1/2$. Third, as the $\ell \approx 1/2$ CDW component has essentially no magnetic field dependence in the narrow range 14–16 T (Fig. 2c), it is possible – by subtraction of Gaussian fits of 14 T diffraction intensities – to isolate the field and temperature dependence of the $\ell = 1$ diffraction intensity.

Superconductivity and CDW phase competition. By subtracting the Gaussian fit of 14 T diffraction intensity from those measured at high fields (see Supplementary Figs. 2 and 3), the temperature dependence of the $\ell = 1$ CDW component at high field is deduced. For both $B = 14.5$ and 15 T, the diffraction intensity is maximum at a finite temperature of $T \approx 25$ K (see Fig. 4). It thus demonstrates that the CDW intensity at $\ell = 1$ has a non-monotonic temperature dependence. This effect can also be analysed from in-plane intensity scans. In Fig. 5a–f, we plot the peak intensity I of Gaussian fits to k -scans through $(0, 4 - \delta_b, \ell)$ as a function of temperature and at magnetic fields as indicated. At $\ell = 1/2$ (Fig. 5), the zero-field temperature dependence

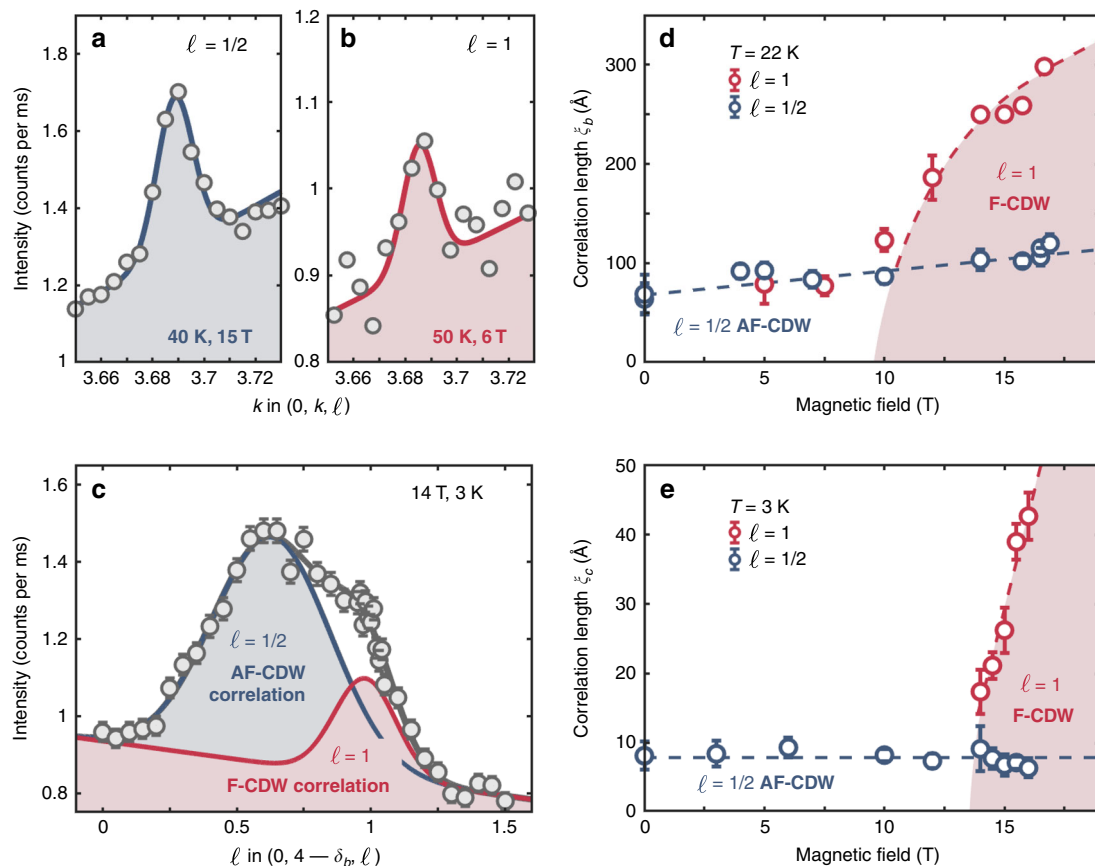


Fig. 3 Two-component analysis of out-of-plane charge-density-wave (CDW) correlations. **a, b** Raw diffraction intensities along $(0, k, 1/2)$ and $(0, k, 1)$ for temperatures and magnetic fields as indicated. **c** Raw diffraction intensity profile along the $(0, 4 - \delta_b, \ell)$ direction, fitted with two Gaussian functions on a linear background. The dark grey line is their sum. **d, e** Magnetic-field-dependent evolution of the respective correlation lengths for $\ell = 1/2$ and 1. The dashed lines and shaded area are guides to the eye. Error bars are standard deviations determined by counting statistics and Gaussian fits, respectively. Source data are provided as a Source Data file.

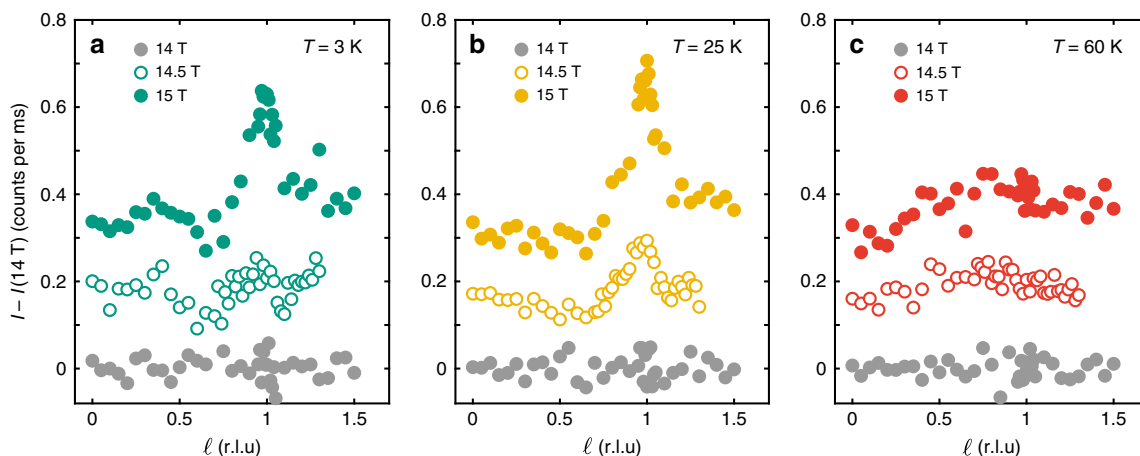


Fig. 4 Temperature and field dependence of in- and out-of-plane diffraction intensities. **a–c** ℓ -dependent diffraction intensity after subtracting the Gaussian fitted $B = 14$ T profiles at temperatures and magnetic fields as indicated. In this fashion, the relative field effects above 14 T are extracted. Raw 14 T ℓ -scans are shown in Supplementary Fig. 2. Data at different fields have been given an arbitrary vertical shift for the sake of presentation. Source data are provided as a Source Data file.

displays a maximum at $T = T_{\max}^{\ell=1/2} = T_c$ – consistent with previous reports^{8,9}. As the magnetic field is increased, $T_{\max}^{\ell=1/2}(B)$ moves to lower temperatures. This effect is found along both a - and b -axis directions (Fig. 5a, b).

The behaviour of the $\ell = 1$ intensity is very different. For low fields, $B \lesssim 10$ T, the field induces a relatively weak response at

$\ell = 1$. It shows a maximum at similar temperature as the $\ell = 1/2$ component (see Fig. 5d). For $10 \lesssim B \lesssim 16$ T, there is a rapid increase of $I(\ell = 1)$ at low temperature (Fig. 5c). The rapid temperature changes below 40 K associated with the crossover field may obscure any maximum due to competition with superconductivity. Then at higher fields $B \geq 14.5$ T, a maximum

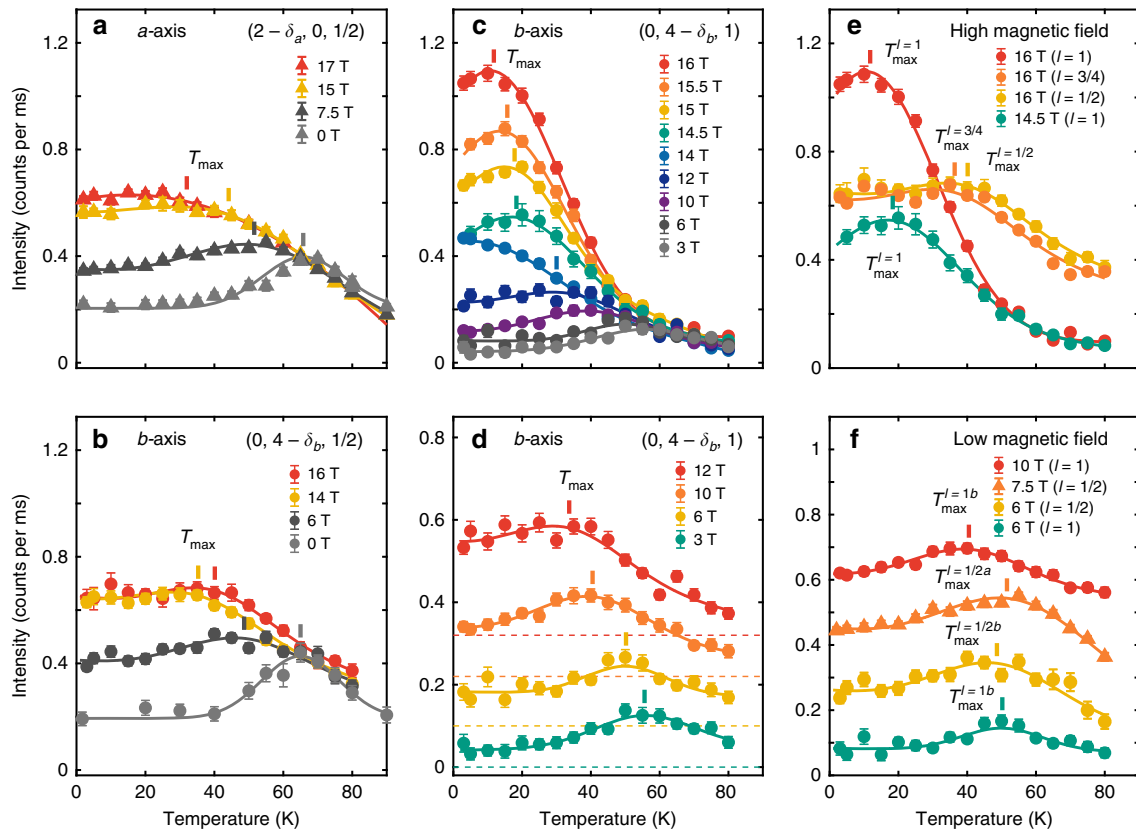


Fig. 5 Temperature scales for phase competition. **a–f** Peak intensities versus temperature measured at $\ell = 1/2$ and 1 charge-density-wave modulation vectors versus temperature. **a, b** Intensity for $(2 - \delta_{a'}, 0, 1/2)$ and $(0, 4 - \delta_{b'}, 1/2)$ with magnetic fields as indicated. Data in **a** and zero-field data in **b** are re-plotted from ref. ⁹. Non-zero magnetic field data in **b** is $\ell = 0.6$ amplitudes obtained from two-Gaussian fits of ℓ -scans. **c** Diffraction intensities at $(0, 4 - \delta_{b'}, 1)$. **d** Same data as in **c** but zoomed on the low-field curves. For visibility, these curves have been given an arbitrary vertical shift - as indicated by the dashed base-lines. **e, f** Comparisons of $\ell = 1$ and $1/2$ temperature dependencies and with that the associated maximum temperature scales T_{\max} for the high- and low- magnetic field regimes respectively. Solid lines are fits to a skewed Gaussian (see text) on a linear background. Vertical bars are the T_{\max} temperature scales defined by the maximum of the second derivative of the skewed Gaussian. Error bars are standard deviations due to counting statistics. Source data are provided as a Source Data file.

again develops at $T_{\max}^{\ell=1}$ which is considerably lower than $T_{\max}^{\ell=1/2}$ for the same field. Direct comparisons of the high- and low-field diffraction intensities at $\ell = 1/2$ and $\ell = 1$ versus temperature are shown in Fig. 5e, f. To extract $T_{\max}^{\ell=1/2}$ and $T_{\max}^{\ell=1}$ in a systematic fashion where the maximum is less well defined, the diffraction intensity versus temperature curves are fitted using a skewed Gaussian function $\Gamma(T) = G(T)[1 + \text{erf}(\alpha T/\sqrt{2})]$ on a linear background (solid lines in Fig. 5). Here $G(T)$ is a Gaussian function and $\text{erf}(\alpha T)$ is the error function. The characteristic temperatures, shown in Fig. 6c versus magnetic field, are derived from the criterion $T_{\max} = \max(-d^2\Gamma/dT^2)$ - this selects either a maximum or saturation point in the diffraction intensity versus temperature. We view T_{\max} as a characteristic temperature scale for competition between CDW and superconducting order.

Correlation lengths. Next, we turn to discuss the CDW correlation lengths. Fig. 3d, e show correlation lengths ξ_b and ξ_c for the lowest temperatures we measured: $T = 22$ and 3 K, respectively. The out-of-plane correlation length $\xi_c^{\ell=1/2} \sim 10$ Å is essentially magnetic-field independent while the in-plane correlation length $\xi_b^{\ell=1/2} \sim 60$ Å increases weakly. This is in strong contrast to the $\ell = 1$ order that gains a dramatic out-of-plane “coherence” above 14 T (Fig. 3e). In fact, $\xi_c^{\ell=1}$ undergoes a fourfold increase from 14 to 16 T. Prior to this change, $\xi_b^{\ell=1}$ increases significantly for field strengths above 10 T (Fig. 3d). Thus at high-fields, the correlation

length of the $\ell = 1$ order exceeds that of the $\ell = 1/2$ CDW component in both in- and out-of-plane directions. It is also interesting to discuss the in-plane correlations at the T_{\max} temperature scales. For $\ell = 1/2$, the correlation length $\xi_b^{\ell=1/2}$ at T_{\max} , is about 20% longer than that at $T = 22$ K in the studied field range (compare Figs. 3d and 6d). The $\ell = 1$ in-plane correlations extend down to zero-magnetic-field (Fig. 6d). At T_{\max} , $\xi_b^{\ell=1}$ exceeds $\xi_b^{\ell=1/2}$ for $B > 5$ T (Fig. 6d), while at 22 K this is only seen at 10 T (Fig. 3d). It is of great interest to note the interplay between the observed peak intensities and the correlation lengths. Our estimates of the k-space integrated intensity for the $\ell = 1$ peak show approximately constant values versus field above 14 T (See Supplementary Fig. 4). This implies that the F-CDW develops longer range correlations with increasing field, but does not increase in amplitude or occupy a significantly larger fraction of the sample volume. The integrated intensity of AF-CDW order does not significantly increase over a range 0–16 T, which leads us to the similar conclusion for the development of AF-CDW.

Discussion

The zero-field maximum at T_c of the $\ell = 1/2$ CDW diffraction intensity has previously been the subject of different interpretations^{9,24–26}. Our view is that the intensity maximum is the result of phase competition between $\ell = 1/2$ CDW order and

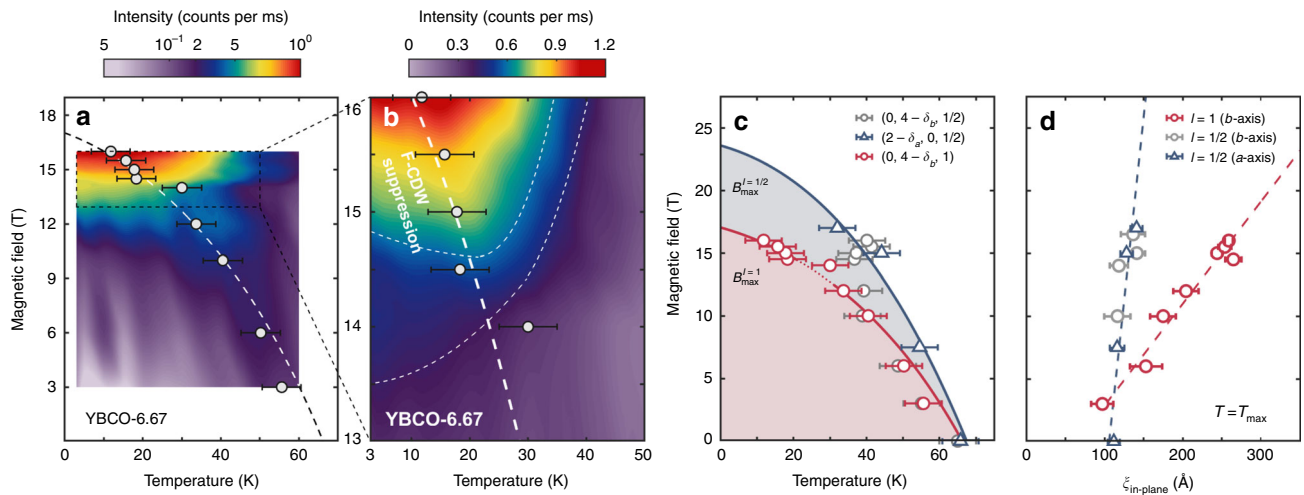


Fig. 6 Competing temperature and magnetic field scales. **a** Intensity map of $(0, 4 - \delta_b, 1)$ (logarithmic colour scale) as a function of temperature and magnetic field. The open circles indicate the temperature scale $T_{\max}^{\ell=1}$ below which suppression of the F-CDW order is observed (Figs. 4a–c). The curved dashed line is a guide to the eye. **b** Intensity map (linear colour scale) focusing on the high-magnetic-field region. The thin dashed lines indicate contour lines. **c** T_{\max} scales inferred from the $\ell = 1/2$ (red) and $\ell = 1$ (blue) charge-density-wave, respectively. Solid lines are guides to the eye. For the $\ell = 1/2$ T_{\max} temperature scale, triangular and circular data points stem from data recorded along the a - (ref. 9) and b -axis (this work) respectively. As the T_{\max} temperature scales indicate the onset of competition with superconductivity, these lines are labelled $B_{c2}^{\ell=1}$ and $B_{c2}^{\ell=1/2}$ in the $T \rightarrow 0$ limit. Error bars indicate the uncertainty related to the determination of the T_{\max} temperature scales. **d** Correlation lengths $\xi_b^{\ell=1/2}$ and $\xi_b^{\ell=1}$ at the respective T_{\max} temperature values. Source data are provided as a Source Data file.

superconductivity. As diffraction intensities are proportional to the square of the CDW order parameter^{23,27}, temperature (or field) dependence reflects the evolution of the CDW order. Upon cooling below T_c , the superconducting order gradually grows, resulting in a partial suppression of the CDW. The balance of this competition can be tipped in favour of the CDW order by application of an external c -axis magnetic field that acts to suppress the superconducting order parameter. With increasing field-strength, the T_{\max} temperature scale shifts to lower values (Fig. 6c) delineating a line in the magnetic field phase diagram that provides a firm lower bound for the border superconductivity and normal state. An approximate extrapolation to the $T \rightarrow 0$ limit yields an upper critical field consistent with that inferred from most bulk measurements^{28–31}. It should be stressed that there is still an ongoing debate about the exact field scale of H_{c2} ³². A similar interpretation can be applied to the temperature dependence of the $\ell = 1$ response. As shown in Fig. 6c, the $\ell = 1$ maximum temperature scale $T_{\max}^{\ell=1}$ is different from T_{\max} for $\ell = 1/2$. This implies the existence of two superconducting onset temperatures at a given applied field or for a fixed temperature two upper critical fields $B_{c2}^{\ell=1/2}$ and $B_{c2}^{\ell=1}$. The different competing temperature and magnetic field scales observed at $\ell = 1/2$ and $\ell = 1$ lend support to our starting hypothesis, namely that there are two different CDW order constituents. In what follows, we discuss the relationship between the CDW and the Fermi surface reconstruction.

It is interesting to consider the implications of our correlation length measurements for the electronic band structure^{33,34}. Although the unfolded structure has not been resolved, the Fermi surface reconstruction (FSR) revealed by quantum oscillation^{35–37} and transport^{38–40} experiments is undoubtedly linked to the appearance of CDW order. It has, however, been debated whether the reconstruction is triggered by the F-CDW or AF-CDW or whether the CDW order is triggered by FSR. The fact that ARPES does not see any FSR⁴¹ has been used as an argument for a field-induced electronic transformation, rather than the reconstruction being already present at zero-field. However, the sign change of the Hall effect persists down to as low as 5 T⁴²,

casting doubt on whether the high-field F-CDW order is responsible for the reconstruction. Recent detailed considerations of CDW correlations concluded that the $\ell = 1$ CDW order has about the right in-plane correlation length to explain the quantum oscillation experiments whereas the AF-CDW correlations are too short³³. We note that at $B = 16$ T the in-plane correlation lengths of the F-CDW and AF-CDW correlations are 300 and 100 Å, respectively. Another signature of FSR is the Hall coefficient which changes sign from positive to negative on cooling^{38–40,43}. It has been demonstrated that for YBCO $p \approx 0.12$, the characteristic sign-changing temperature $T_B = 66$ K $\approx T_c$ is essentially independent of magnetic field³⁸. The sign change in the Hall effect persists down to much lower fields, $B = 5$ T, than the quantum oscillations mentioned above. Thus it is interesting to consider whether the F-CDW correlations might be involved in the FSR at lower fields. We have previously demonstrated¹⁴ that for high magnetic fields, $B = 16.5$ T, $\xi_b^{\ell=1} > \xi_b^{\ell=1/2}$ for $T \approx 66$ K $\approx T_B$. We can see from Fig. 6d that this condition persists at T_{\max} as $B \rightarrow 0$ and $T_{\max} \rightarrow T_B$. In fact, we find that $\xi_b^{\ell=1}$ is longer than $\xi_b^{\ell=1/2}$ down to 5 T where $T_{\max} \approx 55$ K. Thus, F-CDW correlations with $\xi_b^{\ell=1} \geq 100$ Å $\approx \xi_b^{\ell=1/2}$ exist for temperatures $T \lesssim T_B$ and to lowest measured magnetic fields. Considering the (B, T) phase space, both the F-CDW and AF-CDW correlations could be associated with the Fermi surface reconstruction inferred from Hall effect experiments. However, in both cases the correlation lengths are shorter than the expected threshold for quantum oscillations to be observed. Therefore, either the two-dimensionality of the CuO_2 enables the electronic structure to fold also for intermediate correlation lengths or the Fermi surface reconstruction has an entirely different causality and charge order is consequence rather than a trigger.

A central part of this work is the experimental probing of $\ell = 1$ in-plane correlations as a function of magnetic field and temperature. With this, the interaction between $\ell = 1$ CDW order and superconductivity can be discussed. The $\ell = 1$ order displays different competing field and temperature scales, compared to the extensively studied $\ell = 1/2$ order^{8,9,22,23,44,45}. The $T_{\max}^{\ell=1}$ and

$T_{\max}^{\ell=1/2}$ temperature scales indicate the point where superconductivity is strong enough to partially suppress the respective CDW orders. In presence of large enough magnetic fields $B \geq 14$ T, we find that $T_{\max}^{\ell=1} < T_{\max}^{\ell=1/2}$ (Fig. 5e). Extrapolating $T_{\max}^{\ell=1} \rightarrow 0$, a field scale significantly smaller than B_{c2} , inferred from transport measurements^{28,29,40}, is reached. In contrast, $T_{\max}^{\ell=1/2}$ may track B_{c2} at high fields. This suggests that superconductivity occurring in regions with $\ell = 1$ CDW order is weaker than in $\ell = 1/2$ regions. This is especially the case when the $\ell = 1$ correlations develop coherence along the c -axis. The emergence of ferro-coupled long-range $\ell = 1$ CDW order, therefore, induces a fragile state of superconductivity. In the presence of quenched disorder, such a fragile state of superconductivity has, in fact, been predicted theoretically¹⁷. Disorder may therefore play an important role for the organisation of the observed phase diagram^{17,18} and the interaction between CDW order and superconductivity. The exact role of different types of disorder (oxygen-chain vacancies, impurities and vortices) on the AF-CDW order and the fragile superconducting state should be clarified in future experiments. The regime with competition induced weakening of superconductivity has been the setting for predictions of pair-density-wave formations^{3,46–50}. The existence of such a state should manifest itself through a $Q_{\text{PDW}} = Q_{\text{CDW}}/2$ modulation. Although STM studies have reported evidence for PDW order in the halos of vortices⁵¹, there are no x-ray diffraction results supporting the existence of a PDW order in YBCO.

Finally, we comment on the S-shape of B_{DOS} versus temperature reported by density-of-states sensitive probes (specific heat, thermal conductivity, and NMR)⁵². For $B > B_{\text{DOS}}$, the density-of-states is magnetic-field independent and the S-shape, refers to an effect where B_{DOS} , in addition to standard Bardeen-Cooper-Schrieffer (BCS) behaviour, displays a sudden increase in the $T \rightarrow 0$ limit. Our results do not exclude the possibility that $B_{\max}^{\ell=1}$ would increase steeply in the $T \rightarrow 0$ limit. In fact, it is possible that the $\ell = 1/2$ and $\ell = 1$ superconducting flavours couple in the $T \rightarrow 0$ limit to form a uniform condensate. If so, $B_{\max}^{\ell=1}$ and $B_{\max}^{\ell=1/2}$ should merge for $T = 0$. This would lead $B_{\max}^{\ell=1}$ to rise in the low-temperature limit and give it an S-shaped dependence reminiscent of that reported by thermodynamic and spin susceptibility probes of B_{c2} ⁵².

Methods

Experimental details. A high quality single crystal of YBa₂Cu₃O_{6.67} ($T_c = 67$ K) with ortho-VIII oxygen ordering was grown and detwinned as described in ref. ⁵³. Hard x-ray (100 keV) diffraction experiments were carried out, with a horizontal 17 T magnet⁵⁴, at PETRA III's P07 triple-axis diffractometer at DESY (Hamburg, Germany). The YBCO sample was mounted with the magnetic field along the c -axis direction giving access to the $\mathbf{Q} = (h, 0, \ell)$ scattering plane. The setup is identical to that described in ref. ¹⁴, with the exception of an improved sample cooling power allowing a base temperature of $T \approx 3$ K to be reached. Scattering vectors are specified in orthorhombic notation with reciprocal lattice units (r.l.u) ($2\pi/a, 2\pi/b, 2\pi/c$) where $a \approx 3.82$ Å, $b \approx 3.87$ Å, and $c \approx 11.7$ Å.

Data availability

All experimental data are available upon request to the corresponding authors. The source data underlying Figs. 2–6, and Supplementary Figs. 1–4 are provided as a Source Data file.

Received: 17 September 2019; Accepted: 13 January 2020;

Published online: 20 February 2020

References

1. Zaanen, J. & Gunnarsson, O. Charged magnetic domain lines and the magnetism of high- T_c oxides. *Phys. Rev. B* **40**, 7391–7394 (1989).

- Kivelson, S. A. et al. How to detect fluctuating stripes in the high-temperature superconductors. *Rev. Mod. Phys.* **75**, 1201 (2003).
- Berg, E. et al. Dynamical layer decoupling in a stripe-ordered high- T_c superconductor. *Phys. Rev. Lett.* **99**, 127003 (2007).
- Machida, K. Magnetism in La₂CuO₄ based compounds. *Physica C* **158**, 192 (1989).
- Emery, V. J. & Kivelson, S. A. Frustrated electronic phase separation and high-temperature superconductors. *Physica C* **209**, 597 (1993).
- Tranquada, J. M., Sternlieb, B. J., Axe, J. D., Nakamura, Y. & Uchida, S. Evidence for stripe correlations of spins and holes in copper oxide superconductors. *Nature* **375**, 561 (1995).
- Wu, T. et al. Magnetic-field-induced charge-stripe order in the high temperature superconductor YBa₂Cu₃O_y. *Nature* **477**, 191 (2011).
- Ghiringhelli, G. et al. Long-range incommensurate charge fluctuations in (Y,Nd)Ba₂Cu₃O_{6+x}. *Science* **337**, 821 (2012).
- Chang, J. et al. Direct observation of competition between superconductivity and charge density wave order in YBa₂Cu₃O_y. *Nat. Phys.* **8**, 871 (2012).
- LeBoeuf, D. et al. Thermodynamic phase diagram of static charge order in underdoped YBa₂Cu₃O_y. *Nat. Phys.* **9**, 79 (2013).
- Achkar, A. J. et al. Distinct charge orders in the planes and chains of ortho-III ordered YBa₂Cu₃O_{6+d} identified by resonant elastic x-ray scattering. *Phys. Rev. Lett.* **109**, 167001 (2012).
- Wu, T. et al. Incipient charge order observed by nmr in the normal state of YBa₂Cu₃O_y. *Nat. Commun.* **6**, 6438 (2015).
- Gerber, S. et al. Three-dimensional charge density wave order in YBa₂Cu₃O_{6.67} at high magnetic fields. *Science* **350**, 949 (2015).
- Chang, J. et al. Magnetic field controlled charge density wave coupling in underdoped YBa₂Cu₃O_{6+x}. *Nat. Commun.* **7**, 11494 (2016).
- Jang, H. et al. Ideal charge-density-wave order in the high-field state of superconducting YBCO. *Proc. Natl Acad. Sci. USA* **113**, 14645 (2016).
- Kim, H.-H. et al. Uniaxial pressure control of competing orders in a high-temperature superconductor. *Science* **362**, 1040–1044 (2018).
- Yu, Y. & Kivelson, S. A. Fragile superconductivity in the presence of weakly disordered charge density waves. *Phys. Rev. B* **99**, 144513 (2019).
- Caplan, Y. & Orgad, D. Dimensional crossover of charge-density wave correlations in the cuprates. *Phys. Rev. Lett.* **119**, 107002 (2017).
- Comin, R. et al. Charge order driven by Fermi-arc instability in Bi₂Sr_{2-x}La_xCuO_{6+δ}. *Science* **343**, 390 (2014).
- daSilvaNeto, E. H. et al. Ubiquitous interplay between charge ordering and high-temperature superconductivity in cuprates. *Science* **343**, 393 (2014).
- Tabis, W. et al. Charge order and its connection with Fermi-liquid charge transport in a pristine high- T_c cuprate. *Nat. Commun.* **5**, 5874 (2014).
- Blackburn, E. et al. X-ray diffraction observations of a charge-density-wave order in superconducting ortho-II YBa₂Cu₂O_{6.54} single crystals in zero magnetic field. *Phys. Rev. Lett.* **110**, 137004 (2013).
- Hücker, M. et al. Competing charge, spin and superconducting orders in underdoped YBa₂Cu₃O_y. *Phys. Rev. B* **90**, 054514 (2014).
- Liu, Y.-H., Konik, R. M., Rice, T. M. & Zhang, F.-C. Giant phonon anomaly associated with superconducting fluctuations in the pseudogap phase of cuprates. *Nat. Commun.* **7**, 10378 EP (2016).
- Hayward, L. E., Hawthorn, D. G., Melko, R. G. & Sachdev, S. Angular fluctuations of a multicomponent order describe the pseudogap of YBa₂Cu₃O_{6+x}. *Science* **343**, 1336 (2014).
- Nie, L., Sierens, L. E. H., Melko, R. G., Sachdev, S. & Kivelson, S. A. Fluctuating orders and quenched randomness in the cuprates. *Phys. Rev. B* **92**, 174505 (2015).
- Jaramillo, R. et al. Breakdown of the Bardeen-Cooper-Schrieffer ground state at a quantum phase transition. *Nature* **459**, 405 (2009).
- Ramshaw, B. J. et al. Vortex lattice melting and H_{c2} in underdoped YBa₂Cu₃O_y. *Phys. Rev. B* **86**, 174501 (2012).
- Grissonnanche, G. et al. Direct measurement of the upper critical field in a cuprate superconductor. *Nat. Commun.* **5**, 3280 (2014).
- Marcenat, C. et al. Calorimetric determination of the magnetic phase diagram of underdoped ortho ii in YBa₂Cu₃O_{6.54} single crystals. *Nat. Commun.* **6**, 7927 (2015).
- Zhou, R. et al. Spin susceptibility of charge-ordered YBa₂Cu₃O_y across the upper critical field. *Proc. Natl Acad. Sci. USA* **114**, 13148 (2017).
- Yu, F. et al. Magnetic phase diagram of underdoped YBa₂Cu₃O_y inferred from torque magnetization and thermal conductivity. *Proc. Natl Acad. Sci. USA* **113**, 12667 (2016).
- Gannot, Y., Ramshaw, B. J. & Kivelson, S. A. Fermi surface reconstruction by a charge-density-wave with finite correlation length. *Phys. Rev. B* **100**, 045128 (2019).
- Briffa, A. K. R. et al. Fermi surface reconstruction and quantum oscillations in underdoped YBa₂Cu₃O_{7-x} modeled in a single bilayer with mirror symmetry broken by charge density waves. *Phys. Rev. B* **93**, 094502 (2016).
- Doiron-Leyraud, N. et al. Quantum oscillations and the fermi surface in an underdoped high- T_c superconductor. *Nature* **447**, 565 (2007).

36. Sebastian, S. E. & Proust, C. Quantum oscillations in hole-doped cuprates. *Ann. Rev. Condens. Matter Phys.* **6**, 411 (2015).
37. Yao, H., Lee, D. H. & Kivelson, S. Fermi-surface reconstruction in a smectic phase of a high-temperature superconductor. *Phys. Rev. B* **84**, 012507 (2011).
38. LeBoeuf, D. et al. Electron pockets in the Fermi surface of hole-doped high- T_c superconductors. *Nature* **450**, 533 (2007).
39. LeBoeuf, D. et al. Lifshitz critical point in the cuprate superconductor $\text{YBa}_2\text{Cu}_3\text{O}_y$ from high-field Hall effect measurements. *Phys. Rev. B* **83**, 054506 (2011).
40. Chang, J. et al. Nernst and Seebeck coefficients of the cuprate superconductor $\text{YBa}_2\text{Cu}_3\text{O}_{6.67}$: a study of Fermi surface reconstruction. *Phys. Rev. Lett.* **104**, 057005 (2010).
41. Hossain, M. A. et al. In situ doping control of the surface of high-temperature superconductors. *Nat. Phys.* **4**, 527 (2008).
42. Cyr-Choinière, O. et al. Anisotropy of the Seebeck coefficient in the cuprate superconductor $\text{YBa}_2\text{Cu}_3\text{O}_y$: fermi-surface reconstruction by bidirectional charge order. *Phys. Rev. X* **7**, 031042 (2017).
43. Laliberté, F. et al. Fermi-surface reconstruction by stripe order in cuprate superconductors. *Nat. Commun.* **2**, 432 (2011).
44. Blanco-Canosa, S. et al. Momentum-dependent charge correlations in $\text{YBa}_2\text{Cu}_3\text{O}_{6+\delta}$. *Phys. Rev. Lett.* **110**, 187001 (2013).
45. Blanco-Canosa, S. et al. Resonant x-ray scattering study of charge-density wave correlations in $\text{YBa}_2\text{Cu}_3\text{O}_{6+x}$. *Phys. Rev. B* **90**, 054513 (2014).
46. Agterberg, D. F. et al. The physics of pair density waves. Preprint at <http://arxiv.org/abs/1904.09687> (2019).
47. Agterberg, D. F. & Tsunetsugu, H. Dislocations and vortices in pair-density-wave superconductors. *Nat. Phys.* **4**, 639 (2008).
48. Pépin, C., de Carvalho, V. S., Kloss, T. & Montiel, X. Pseudogap, charge order, and pairing density wave at the hot spots in cuprate superconductors. *Phys. Rev. B* **90**, 195207 (2014).
49. Dai, Z., Zhang, Y., Senthil, T. & Lee, P. A. Pair-density waves, charge-density waves, and vortices in high- T_c cuprates. *Phys. Rev. B* **97**, 174511 (2018).
50. Wang, Y. et al. Pair density waves in superconducting vortex halos. *Phys. Rev. B* **97**, 174510 (2018).
51. Edkins, S. D. et al. Magnetic field-induced pair density wave state in the cuprate vortex halo. *Science* **764**, 976 (2019).
52. Kačmarčík, J. et al. Unusual interplay between superconductivity and field-induced charge order in $\text{YBa}_2\text{Cu}_3\text{O}_y$. *Phys. Rev. Lett.* **121**, 167002 (2018).
53. Liang, R., Bonn, D. A. & Hardy, W. N. Growth of YBCO single crystals by the self-flux technique. *Philos. Mag.* **92**, 2563 (2012).
54. Holmes, A. T., Walsh, G. R., Blackburn, E., Forgan, E. M. & Savey-Bennett, M. A 17 T horizontal field cryomagnet with rapid sample change designed for beamline use. *Rev. Sci. Instrum.* **83**, 023904 (2012).

Acknowledgements

We acknowledge informative discussions with Steve Kivelson. This work was supported by the EPSRC (grant numbers EP/R011141/ & EP/J016977/1), the U.S. Department of

Energy (DOE), under Contract No. DE-AC02-98CH10886, the Wolfson Foundation, the Royal Society, the Office of Basic Energy Sciences, Division of Materials Science and Engineering, the Danish Agency for Science, Technology and Innovation under DAN-SCATT, the Leverhulme Trust, and the Swiss National Science Foundation. Parts of this research were carried out at beamline P07 at DESY, a member of Helmholtz Association HGF.

Author contributions

R.L., D.A.B. and W.N.H. grew and characterised the $\text{YBa}_2\text{Cu}_3\text{O}_{6.67}$ single crystal. E.B., O.I., A.T.H., N.B.C., M.H., E.M.F., O.G., U.R., M.v.Z., S.M.H. and J. Chang executed the x-ray diffraction experiments. J. Choi, O.I., S.G., S.M.H. and J. Chang analysed the data. All authors contributed to the manuscript. J. Choi and O.I. equally contributed to this work.

Competing interests

The authors declare no competing interests.

Additional information

Supplementary information is available for this paper at <https://doi.org/10.1038/s41467-020-14536-1>.

Correspondence and requests for materials should be addressed to S.M.H. or J.C.

Peer review information *Nature Communications* thanks Jun-Sik Lee and the other, anonymous, reviewer(s) for their contribution to the peer review of this work. Peer reviewer reports are available.

Reprints and permission information is available at <http://www.nature.com/reprints>

Publisher's note Springer Nature remains neutral with regard to jurisdictional claims in published maps and institutional affiliations.



Open Access This article is licensed under a Creative Commons Attribution 4.0 International License, which permits use, sharing, adaptation, distribution and reproduction in any medium or format, as long as you give appropriate credit to the original author(s) and the source, provide a link to the Creative Commons license, and indicate if changes were made. The images or other third party material in this article are included in the article's Creative Commons license, unless indicated otherwise in a credit line to the material. If material is not included in the article's Creative Commons license and your intended use is not permitted by statutory regulation or exceeds the permitted use, you will need to obtain permission directly from the copyright holder. To view a copy of this license, visit <http://creativecommons.org/licenses/by/4.0/>.

© The Author(s) 2020